PCCP

ROYAL SOCIETY OF CHEMISTRY

PERSPECTIVE

View Article Online
View Journal | View Issue

Cite this: *Phys. Chem. Chem. Phys.*, 2023, **25**, 17092

Catalytic enhancement of production of solar thermochemical fuels: opportunities and limitations

Juan M. Coronado * and Alicia Bayón

Solar thermochemical fuels are a promising low-carbon alternative to conventional fossil fuels, which must be swiftly phased out to mitigate the consequences of climate change. Thermochemical cycles powered by concentrating solar energy at high temperatures have demonstrated efficiency in the conversion of solar to chemical energy exceeding 5% and have been assayed in pilot scale facilities of up to 50 kW. This conversion route implies the use of a solid oxygen carrier that enables CO_2 and H_2O splitting, generally operating in two consecutive stages. The primary product of the combined thermochemical conversion of CO_2 and H_2O is syngas (CO + H_2), which for practical applications must be catalytically transformed into hydrocarbons or other chemicals such as methanol. This link between thermochemical cycles, involving the transformation of the whole solid used as an oxygen carrier, and catalysis, occurring only on the material surface, calls for exploitation of the synergies between these two unlike but interconnected gas–solid processes. Accordingly, in this perspective we discuss the differences and similitudes between these two transformation routes, consider the practical impact of kinetics in thermochemical solar fuel generation and explore the limits and opportunities of the catalytic promotion. With this aim, first, the potential benefits and hurdles of direct catalytic enhancement of CO_2 and H_2O dissociation in thermochemical cycles are discussed and then, the possibilities of improving the catalytic production of hydrocarbon fuels, basically methane, are also assessed. Finally, an outlook of the future opportunities of the catalytic promotion of thermochemical solar fuel productions is also provided.

Received 7th February 2023,
Accepted 30th May 2023

DOI: 10.1039/d3cp00609c

rsc.li/pccp

Introduction. Sustainable solar fuels for an imminent future

The increasing awareness in the society about the risks of climate change, which is causing growing environmental and economic concerns, is placing decarbonization of energy at the focal point of challenges faced by humankind. Although global agreements such as that reached at COP26 in Glasgow in 2021 are necessary to deal with this worldwide endeavor, the scientific community must develop a broad portfolio of viable technical solutions to swiftly reduce the carbon footprint of energy.

Increasing efficiency in energy consumption and promoting the use of renewable sources are the basic keystones of the new emerging energy panorama. Currently, the electrical grid is increasingly renewable, with the largest deployment of new generation plants in China, USA, Brazil, India and the European Union. In contrast, climatization, including both air-conditioning and heating systems, together with industrial applications are still globally based on fossil resources (>85% in 2019), while oil-based liquid fuels constitute more than 95% of the world's energy share in the transport sector.[1]

To progress in this direction, a number of routes for the production of more sustainable synthetic fuels powered by different renewable sources are currently being investigated.[2,3] Solar fuel production is particularly promising because it allows storage of solar energy in chemical bonds. This can be achieved by following different transformation routes (see Fig. 1), such as photocatalysis, photoelectrochemical or thermochemical. The primary product of most of these transformations is hydrogen, which is attracting a huge deal of interest due to the versatility of this simple molecule as an energy vector, with applications in fuel cells and adapted engines.[4] Furthermore, hydrogen is also an essential reagent in the chemical industry, and it can enable CO_2 valorisation to produce fuels and chemicals, providing a potential way to reach neutral or even negative carbon emissions.[5]

The technical readiness levels of these technologies vary widely, but generation of green (CO_2-free) hydrogen by electrochemical

Instituto de Catálisis y Petroleoquímica. ICP-CSIC. C/Marie Curie, 2. E-28049. Madrid, Spain. E-mail: jm.coronado@csic.es

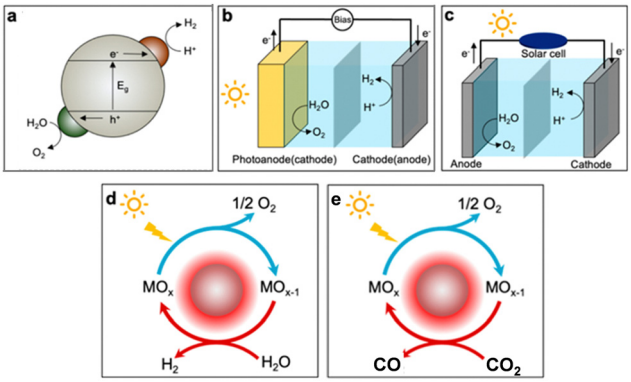

Fig. 1 Main routes to produce solar fuels: (a) photocatalytic (PC), (b) photoelectrochemical (PEC), and (c) photovoltaic–electrochemical (PV-EC) water splitting; solar thermochemical (STC) (d) water and (e) CO_2 splitting. Adapted from ref. 2 with permission from the American Chemical Society.

water splitting externally powered by wind or photovoltaic (PV) electricity is already on the verge of commercial exploitation. A usual metric to determine how much energy can be chemically stored is the solar-to-hydrogen (STH) efficiency, which is calculated as the ratio between the hydrogen rate and the solar irradiance multiplied by the exposed area of the device. For PV systems this parameter can exceed 30% in some optimized systems based on triple-junction solar cells.[2,6] Yet, using commercially available crystalline Si cells coupled with optimized electrodes of Pt and $WO_{2.72}$ co-doped with Co and Fe, and operating in alkaline media, an average solar-to-hydrogen efficiency of 16.9% was achieved during 50 h of operation.[7] These selected examples of high yields illustrate the foremost position of this technology to commercially deliver carbon-free hydrogen. In spite of this, the price of this green hydrogen, with values expressed as the levelized cost of hydrogen (LCOH) ranging from 6 to 2 $ per kg, is still higher than that produced industrially by the steam reforming of methane (generally lower than 2 $ per kg), although economically competitive production is estimated to be achievable in few years.[8]

Research on alternative transformation schemes to those based on electrolysers powered by PV (Fig. 1c) and directly activated by sunlight in a single step is gathering notable interest due to their potential to achieve high energy conversion yields. Among these technologies, photoelectrochemical water splitting (see Fig. 1b) is leading the way because of its competitive efficiency for hydrogen production.[2,9] Solar-to-hydrogen efficiencies higher than 19% were obtained in acidic media using a device with an Rh-based photoelectrocatalyst on a complex multi-layered semiconductor structure.[10] For photocatalysis, which is exclusively activated by light (Fig. 1a), the best results were achieved using carbon nanodots dispersed STH on C_3N_4 as the photocatalyst. This system reaches only 2% of water splitting without using any sacrificial agent.[11] Recently, an STH efficiency of 9% has been reported for water splitting using InGaN/GaN nanowires as photocatalysts with a complex co-catalyst containing Rh, Cr and Co and operating at about 70 °C under sunlight irradiation.[12] This increment in the temperature appears to be instrumental to achieve higher hydrogen yields and points out the relevance of exploring photothermal approaches, based on simultaneous thermal and photonic activation, for energy and other applications.[13]

Thermochemical solar fuels (Fig. 1d and e) have already reached interesting energy yields that exceed 5% solar to fuel conversion,[14] and they present a large theoretical potential for additional improvement. Recently, thermochemical hydrogen generation has proved to be comparable with photoelectrocatalytic hydrogen production in efficiency, providing an attractive option for those locations with high direct irradiation.[15] In addition, this technology is well adapted to complement electricity generation in concentrating solar plants[16] and it also allows a very selective CO_2 splitting, which is not easily achieved by other technologies. However, the thermochemical route for solar fuel production is not free of drawbacks, because the requirement of operating at high temperature adds complexity to thermochemical reactors and demand thermally resistant materials that can increase the cost of the commissioning of these plants. In addition, these systems are less adapted to modular deployment than the other technologies based on direct activation by photons and need extensive heliostat fields to reach reasonable productivity.

A more detailed vision of the current state of the art of this technology, with emphasis on material development, is given in the next section.

Thermochemical solar fuels production

Currently, most of the research on solar thermochemical fuels is focussed on cycles of two stages, that involve separate and consecutive reactions that when combined lead to H_2O or CO_2 splitting. This is achieved with the assistance of an oxygen carrier, which generally is a redox metal oxide (see Fig. 2). The corresponding reactions of this stepwise process using a generic reducible non-stoichiometric oxide, MO_x, are the following:

$$MO_x \rightleftharpoons MO_{x-\delta} + \delta/2\ O_2 \quad (1)$$

$$MO_{x-\delta} + \delta\ H_2O \rightleftharpoons MO_x + \delta\ H_2 \quad (2)$$

$$MO_{x-\delta} + \delta\ CO_2 \rightleftharpoons MO_x + \delta\ CO \quad (3)$$

In these equations, δ represents the non-stoichiometric coefficient, which is related to the amount of oxygen released from the solid in the reduction step, as shown in eqn (1). Lowering the oxygen partial pressure and working at high temperatures shift the equilibrium of reaction (1) to the right and allows maximizing the required reduction degree. Accordingly, reactors for thermochemical cycles exclude oxygen either using an inert gas carrier, commonly employed in lab scale tests, or operating under vacuum. This last procedure is often applied in upscaled plants for avoiding the cost and the energy penalty of the separation of the products from the inert gas stream.

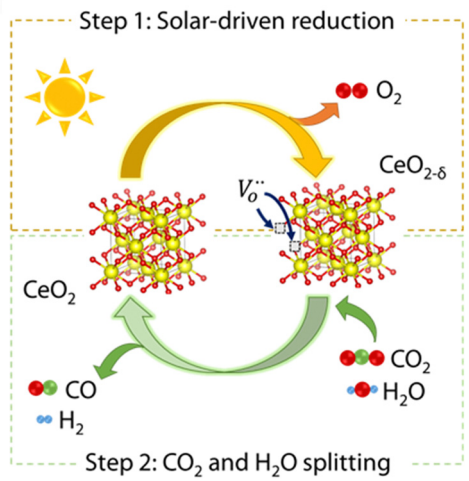

Fig. 2 Scheme of the thermochemical cycle for CO_2 and H_2O splitting over CeO_2. Reproduced with permission from ref. 26 with permission from RSC.

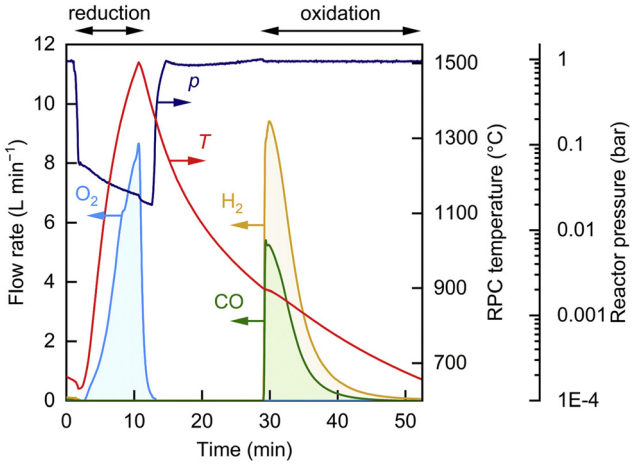

Fig. 3 Time evolution of the temperature, reactor pressure, and flow rates of the gas products (O_2, CO, and H_2) during a representative redox cycle using an alveolar foam of CeO_2 (18.1 kg) and with a mean P_{solar} = 42.0 ± 6.2 kW. Reproduced with permission from ref. 17 with permission from Elsevier.

In the second stage, two differentiated paths for reoxidation of the oxygen carrier can be considered as indicated in eqn (2) and (3), by using either H_2O to produce H_2 or CO_2 to obtain CO. In practice, coprocessing of H_2O and CO_2 mixtures is the preferred option, because the outcome is the blend of H_2 and CO, known as syngas, which can be fed to a second catalytic unit in 2:1 proportion to produce synthetic fuels using Fischer–Tropsch technology.[17] Besides, the synthesis of methanol from solar syngas with a H_2/CO ratio higher than 3 has been also explored.[18] Thermodynamic dictates that H_2O and CO_2 splitting reactions are more efficient at lower temperatures than those previously applied for vacancy formation. Therefore, efficient isothermal operation of these cycles, although preferred to avoid heat losses, is difficult to implement in practice.

Thermochemical cycles with three or more stages, such as H_2SO_4–SO_x or MnO–Na_2CO_3,[19,20] have also been investigated due to their potential for achieving high hydrogen yields. However, the increasing complexity of the required reactors, the concerns about material corrosion as well as the challenges of efficient heat recovery caused by the significant temperature gap between the different reaction stages have limited the interest of these cycles for solar applications.

Several redox oxides have been studied as possible oxygen carriers for high temperature thermochemical cycles, although research is currently focussed on the use of perovskites and CeO_2, because these materials showed promising efficiencies. In the case of CeO_2, despite the initial attempts to deal with the fully reduced oxide, Ce_2O_3, the extreme temperatures (*ca.* 2000 °C) required for this transformation hindered achieving complete conversion.[21] In contrast, the use of partially reduced ceria, $CeO_{2-\delta}$, has proved to be more successful, and the seminal article of Chueh *et al.* published in 2010 unveiled the remarkable performance of CeO_2 as an efficient oxygen carrier due to its favourable thermodynamics.[22] Typically, as it is shown in the graph of Fig. 3, thermochemical production of syngas on CeO_2 occurs by reduction of the solid at 1500 °C with a p_{O2} lower than 0.02 bars, and subsequent reoxidation by introducing a mixture of steam and CO_2 in the reactor at about 900 °C.

The unparallel reduction entropy of CeO_2, which is mostly associated with the contribution of the configurational entropy of the f electrons of the lanthanide group,[23] is a key aspect to explain the notable thermochemical activity of CeO_2. Subsequent investigations by the Steinfeld group, using a larger scale reactor with CeO_2 shaped as reticulated foams, have set the record on sun-to-fuel efficiency of 5.25% for the thermochemical CO_2 splitting at non-isothermal conditions.[14] This system achieved a CO_2 conversion of 83% and showed stability for 500 cycles under a concentration of 3000 suns provided by a solar simulator of 4 kW. Recently, thermochemical hydrocarbon fuel production has been demonstrated at a much larger scale reactor (50 kW) powered by a modular 500 m^2 heliostat field.[17] This system was fed with a mixture of CO_2 and H_2O vapor and, under realistic operation conditions with real sunlight, reached an efficiency of 4.1% for syngas production (see Fig. 3), which is slightly lower than that of the bench-scale prototype. This work has established that despite the complexity of operating with high solar fluxes and at elevated temperatures, deployment of plants for thermochemical fuel production is feasible with medium-sized plants with high concentrations (about 2500 suns) and located in areas with moderate solar irradiance.

Several attempts to enhance the thermochemical performance of CeO_2 by introducing additional metals have been reported. Doping ceria with up to 20% mols of Zr allows doubling the hydrogen production by increasing the reducibility of the mixed $Ce_{1-x}Zr_xO_2$ oxide, which retains the fluorite structure.[24] However, to fully exploit this higher hydrogen generation capacity is necessary to increment the water vapor concentration to compensate for the slower re-oxidation kinetic of the doped material. Similarly, enhancement of the CO_2 splitting activity for ceria doped with

15% of Hf has also been reported but, as in the case of Zr, at the cost of sluggish hydrogen evolution.[25] Morphology of the solid is also important for easing the gas–solid contact and to allow a better distribution of the incident solar radiation. Accordingly, CeO_2 has been used as porous fibres or as alveolar foams in larger scale reactors.

Perovskites, with the general formula ABO_3 have been proposed as potentially suitable oxygen carriers due, among other reasons, to their noteworthy chemical adaptability. The crystalline lattice of perovskites is theoretically cubic, although distortions leading to tetragonal or hexagonal symmetries are common. Perovskites are characterized by their chemical versatility that allows them to accommodate a number of different cations on both A and B sites, as long as the electroneutrality and the geometric constraints of the lattice are preserved.[26,27] In this respect, the large cation A must fit in a 12-fold coordinated site, while the B element occupies an octahedral one. Furthermore, if the cation B, or less frequently that in A site, is redox active, perovskites can undergo partial oxygen release at high temperatures and low oxygen partial pressure, yielding the reduced oxide $ABO_{3-\delta}$.

This reactivity can be exploited in thermochemical cycles. In this way, perovskites of the family $La_{1-x}Sr_xMnO_3$ have been proved to be active for water and CO_2 splitting with higher efficiency than CeO_2 and at lower temperatures.[28] Additional doping of the B site results in oxides such as $La_{0.6}Sr_{0.4}Mn_{0.4}Al_{0.6}O_3$ that present an attractive performance for CO_2 and H_2O splitting.[29,30] Just to give an impression about the chemical diversity of perovskite compositions so far investigated, but without trying to be exhaustive, recent reports have also shown promising thermochemical activity of $CaTi_{0.5}Mn_{0.5}O_3$[31] and $BaCe_{0.25}Mn_{0.75}O_3$[32] for hydrogen production and of $La_{0.6}Sr_{0.4}Cr_{1-x}Co_xO_3$[33] for CO generation. Furthermore, some composite systems using perovskites and CeO_2 have also been investigated to take advantage of the possible synergies between the two redox components.[34] Besides, *ab initio* calculations using Density functional theory (DFT) has emerged as a very convenient theoretical tool to determine the thermodynamic properties of a large number of perovskites and to identify chemical compositions with high potential efficiency.[35] For additional information on the application of perovskites to solar thermochemical fuel production, the readers are referred to the excellent specific reviews on this topic.[27,36]

Mixed oxides of other structural families different than perovskites can be also applied to thermochemical water splitting. Notably, Ni ferrites, $NiFe_2O_4$, have widely been investigated for this application, and those doped with Zn were successfully used at large scale (100 kW) for solar hydrogen production, although they showed low cycling stability.[37] Besides, Ni ferrites have also proved to be active for CO_2 splitting at the lab scale.[38] More recently, mixed oxides containing four different transition metals, Ni, Fe, Mg and Co, and consisting of a mixture of rock salt and spinel structures have demonstrated considerable water splitting activity at temperatures below 1100 °C.[39] These results show a wide range of chemical compositions of metal oxides that can be explored as potential oxygen carriers. This is prompting the application of data science tools such as machine learning for the selection of appropriate candidates for oxygen carriers.[40]

For establishing the potential applicability of a specific material for production of solar thermochemical fuels, their thermodynamic functions for vacancy formation, both enthalpy and entropy, should be determined as a function of temperature, pressure, and non-stoichiometry. As mentioned earlier, these parameters can be obtained by DFT calculations, but validation of theoretical values requires careful, systematic and time-consuming experimental work.[41] Easy reducibility of the redox oxides according to eqn (1) can be positive for achieving high non-stoichiometry, but the key aspect for the applicability of a redox material in thermochemical cycles is whether it can supply the energy necessary to drive H_2O and CO_2 splitting during the subsequent stage when the solid is reoxidated. Therefore, a specific material can be utilized for thermochemical fuel production under a fixed set of conditions of pressure, temperature and gas composition only if $\Delta G < 0$ for the processes described in eqn (2) and (3). Recently, Bayón *et al.* have systematized these thermodynamics calculations to determine the viability of using specific perovskite compositions and considering directly the enthalpy and entropy of oxygen vacancy formation, as illustrated in the graph of Fig. 4.[42] Similarly, Haile and co-workers have explored the expected limits of the solar-to-fuel efficiency that can be reached considering fixed bed reactors by using an

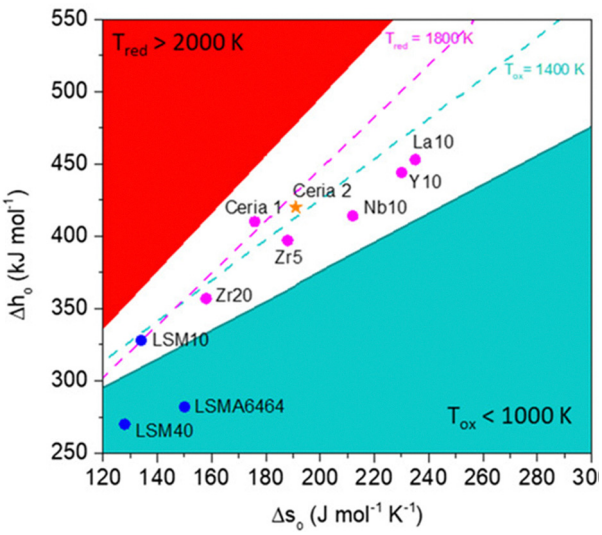

Fig. 4 Graphs plotting the enthalpy of oxygen vacancies formation, Δh_o, as a function of the entropy, Δs_o, of selected redox oxides used in thermochemical cycles to reach $\Delta g_o = 0$. Fixed oxygen partial pressure ($p/p_0 = 10^{-5}$) and 10% of conversion were considered for a fixed range of temperatures for the reduction (solid red and dashed pink lines) and water splitting (blue solid and dashed lines) equilibrium. The white area represents values of the thermodynamic properties with operation temperatures judged reasonable for solar thermal applications. This region is delimited for reduction below 2000 K (higher temperatures appear in the red sector) and reoxidation above 1000 K (blue area), while for reoxidation between 1800 and 1400 K is the white space between dashed lines. Dots represent values of selected materials used as oxygen carriers. Reproduced with permission from ref. 42 with permission from Wiley.

iterative method and applying quasi-equilibrium conditions to some selected oxides.[43] These results predict a solar-to fuel energy yield of 12.9% at a CeO_2 reduction temperature of 1500 °C, while the estimated efficiency for other potentially promising materials under realistic operation conditions is lower, including that of the Zr-doped CeO_2 (10.1%) and $La_{0.8}Sr_{0.2}MnO_3$ perovskite (3.3%). So far, perovskites cannot compete with the efficiencies of CeO_2 when performing a side-to-side comparison,[44] although considering the immense number of possible compositions of those mixed oxides, there is significant expectation of finding novel materials that could outperform CeO_2.

Isothermal operation of both reduction and oxidation stages can provide advantages in terms of limiting heat losses, which is the main contribution to decreasing the efficiency in thermosolar processes.[15] In this respect, considering the thermodynamic functions, it has been estimated that the potential solar-to-fuel efficiency for CeO_2 could reach up to 28% by implementing an optimized heat recovery system.[45,46]

In addition to thermodynamic considerations, experimental studies have shown that thermodynamic properties do not fully account for the suitability of redox materials to produce solar thermochemical fuels, because unfavourable kinetic may turn impractical in the use of materials with satisfactory redox properties. This is particularly relevant during the CO_2 and water splitting because this stage generally occurs at lower temperatures, reducing the reaction driving force. These aspects have been highlighted in many experimental studies and partially considered in the recent model by Haile's group.[43] Pure ceria presents slow reduction kinetics and relatively fast reoxidation, while perovskites and doped ceria are faster during reduction and slower during the reoxidation of the solid which takes place during the water splitting reaction.[47] To cope with these constraints, the concentration of the gas reagents, CO_2 and water is frequently increased to compensate for the slow reoxidation rate. However, this strategy has a negative impact on the overall efficiency of the process because the energy required for heating larger volumes of gas and the lower efficiency of separation of the products from the unreacted molecules impose an important penalty on the energy that can be accumulated on products.[15] This calls for additional approaches to boost the rate of syngas production, as explored in the following sections.

The relevance of kinetics for thermochemical cycles

Due to the impact of kinetic on the productivity of solar fuels, different empirical and theoretical approaches have been used to understand the key parameters determining the rate of thermochemical cycles. This section summarizes the main research efforts in this area.

The master plot method, which considers different equations for solid state kinetic in a normalized graph, has been applied to analyze the kinetic of thermochemical cycles.[48] Results of this approach suggest that CO_2 splitting over $Zr_{0.25}Ce_{0.75}O_2$ is controlled by diffusion within the solid, while water splitting appears to follow a first-order kinetic. However, the agreement between experimental data and model predictions is far from perfect, particularly for low conversion of the redox material. In contrast, good matching of hydrogen generation over pure CeO_2 was obtained by fitting experimental data with a model considering a first-order deceleration of the rate.[49] Similarly, hydrogen production by water splitting over Zr-modified ceria, or co-doped with Zr and Gd or Pr, was reproduced by applying a power-law decelerating kinetic. To select the most appropriate model, an iterative algorithm was used to determine which model of solid-state kinetics better matched the experimental results.[50] This approach suggests that water splitting is controlled by surface reaction rather than by diffusion in the bulk. A simple analytical model was proposed by Bulfin *et al.* with the aim of explaining the reduction and oxidation kinetics of ceria with O_2,[51] and it was lately applied to Zr-doped ceria.[47] This method considers the rate of variation of the concentration of oxygen vacancies and assumes thermodynamic equilibrium to reproduce the experimental oxygen release and uptake curves. From these results, the authors concluded that doped materials showed slower kinetics than pure ceria.[47] However, the reduction reaction seemed to be limited by the heating rate, despite being extremely high. These results stress the importance of considering not only the effect of the kinetic on the chemistry of the redox material but also the physical parameters affecting mass and heat transport.

In contrast with previous approaches, the so-called thermo-kinetic model poses that the rate of the two stages of water splitting can be described satisfactorily considering only the independently determined thermodynamic properties, without including any fitting parameters.[52,53] This model, extensively investigated by Haile's group, stated that thermodynamic equilibrium at high enough operation temperature is reached so rapidly that the rate of the process is defined only by the flow of reagents and products at the operation conditions.[54–56] This implies that both surface reaction and oxygen diffusion through the solid are considered to occur so rapidly that they do not have a measurable effect on the overall kinetics. Therefore, the only constrains to the reactivity of the redox solid are their thermodynamic properties and the effective activation energy approaches zero. Therefore, by applying a mass balance to the inlet and outlet streams, analytic equations can be obtained for water splitting that depends only on the thermodynamic properties of the oxygen carrier and selected conditions of gas composition, flow rate and temperature. Following this method, experimental results of water splitting over CeO_2 and perovskite $La_{1-x}Sr_xMnO_3$ were adequately reproduced under different operation conditions. Generally, a good agreement between experimental results and the predictions of the thermo-kinetic model is obtained, but significant deviations are observed for CeO_2 at the lower temperatures when the assumptions of the model do not fully hold. Similarly, an appreciable mismatch with this quasi-equilibrium model is observed for water splitting over the perovskite $CaTi_{0.5}Mn_{0.5}O_3$, particularly at the beginning of the water splitting stage, due to

Table 1 Summary of the kinetic models applied to the thermochemical cycles for solar fuel production

Reaction	Sample	Equipment	Methodology	E_a (kJ mol^{-1})	Model	Ref.
CDS	$Zr_{0.25}Ce_{0.75}O_2$	TGA	Master plot	82–103[a]	Diffusion	47
WS	CeO_2	SFR	Model fitting	29[b]	First order decelatory	48
WS	CeO_2 doped with Zr, Gd or Pr	SFR	Model fitting	—	Power law	49
WS	CeO_2	CFR	Prediction based on thermodynamics	—	Thermo-kinetic	52 and 53
WS	$La_{1-x}Sr_xMnO_3$	CFR	Prediction based on thermodynamics	—	Thermo-kinetic	54
OR	$Ce_{1-x}Zr_xO_2$ & CeO_2	XLV	Fitting to the experimental esults	26–30 ± 2.5 ($Ce_{1-x}Zr_xO_2$)[a] 36 ± 4 (CeO_2)[a]	Based on vacancies equilibrium & diffusion/shrinking Core	46 and 50
WS	CeO_2	CFR	Fitting to the experimental results	190 ± 50[b]	Based on vacancies and electrons equilibrium & transport	56

TGA: thermogravimetric analyzer, SFR: stagnation flow reactor, XLV: Xenon Lamp in Vacuum chamber, CFR: continuous flow reactor, OR: re-oxidation in O_2. [a] Estimated by Arrhenius plot from experimental data obtained at different temperatures. [b] Calculated by the multiparametric fitting of the kinetic model to the experimental data.

the kinetic limitations of the material.[30] In this way, experimental time-resolved studies carried out by means of the electrical conductance relaxation method show that the thermo-kinetic regime provides a good description at relatively low flow rates, high temperatures and large surface area of the oxide.[51]

Alternatively, detailed defect analysis considering the migration of oxygen vacancies from the bulk to the surface was used to reproduce the experimental hydrogen production over CeO_2 by fitting the thermodynamic parameters of vacancy formation and the corresponding kinetic constants.[57] Table 1 summarizes the main kinetic studies included in this review.

In addition to the intrinsic characteristics of the redox materials, their textural properties have also an important impact on kinetic. This has been shown for CO_2 splitting with CeO_2, which when used as a tridimensional ordered microporous (350–50 nm) material presents a rate one order of magnitude larger than for the non-porous oxide.[58]

The study of the mechanism of reoxidation of the redox oxides by water vapor and CO_2 can be approached by means of DFT calculations. Wolverton *et al.* showed that the dissociation of water on oxygen vacancies of CeO_2(111) to yield surface hydroxyls presents an insignificant energy barrier.[59] However, for an efficient H_2 release, it is proposed that the most efficient pathway implies the reaction of Ce–H species with the Ce–OH surface group. This route proceeds with an estimated activation energy of about 110 kJ mol^{-1} (1.14 eV barrier). In contrast, other studies of CeO_2 proposed Ce–OH species as intermediate for the desorption of H_2, although with great differences in the calculated energy barrier. Thus, in one report formation of H_2 present an activation energy of about 400 kJ mol^{-1},[60] which is much larger that for water desorption, while a more moderate barrier of about 200 kJ mol^{-1} was determined in other DFT studies.[57] More recently, the reaction of surface vacancies on $Ce_{0.75}Zr_{0.25}O_2$(111) with water was also studied by DFT. The results obtained revealed that hydrogen generation occurs in two steps, first water dissociation on the surface oxygen vacancies and then the migration of a hydrogen atom to yield two hydroxyls, which subsequently react to release H_2. The activation energies of these two processes are 84.5 kJ mol^{-1} and 169.2 kJ mol^{-1}, respectively.[61] DFT calculations for Nb-doped CeO_2 suggested a similar pathway with an activation energy of 64 kJ mol^{-1} for hydrogen transfer and 154 kJ mol^{-1} for H_2formation.[62] Other DFT studies of Zr and Pr doped ceria also confirmed that desorption of H_2 is the rate-limiting stage with energy barriers around 2 eV.[50] These theoretical energy barriers are within the high-end of the values determined experimentally for water splitting, as listed in Table 1, which show a significant dispersion, with energies varying in the 80–200 kJ mol^{-1} range.

On the other hand, CO_2 interaction on reduced $Ce_{0.75}Zr_{0.25}O_2$(111) leads to the adsorption of CO_2 on an oxygen vacancy and the formation of the adsorbed carbonyl with an activation energy of 72.9 kJ mol^{-1} (see Fig. 5). The DFT results obtained for unmodified CeO_2(111) in these two processes are similar although the activation energies are slightly higher. These theoretical energy barriers are slightly higher than those experimentally determined from Arrhenius plots, which were in the 80–105 kJ mol^{-1} range for CO_2 splitting using $Zr_{0.25}Ce_{0.75}O_2$, although the accuracy of these values is limited by the small number of tests performed.[48]

Fast kinetic implies having a very low activation energy process, which appears to be the case for oxygen release at high temperatures, but both theoretical and experimental reports indicate that dissociation of CO_2 and water on reduced oxide surfaces present a significant energetic barrier. This implies that under the operation temperatures required for CO_2 and H_2O dissociation, the rate for the generation of both CO and H_2 is lower than expected by the thermodynamics limit. Catalytic promotion can provide an opportunity for overcoming the kinetic constrains of solid re-oxidation. This is because catalysts can potentially offer alternate reaction pathways with lower activation energy, increasing the rate for the generation of H_2 and CO. Therefore, catalysis holds the promise of being a game changer for materials such as many perovskites, which show kinetic limitations at the low-temperature stage of fuel production.

Critically reviewing the relevance of catalysis in thermochemical solar fuels generation, considering the reasons for

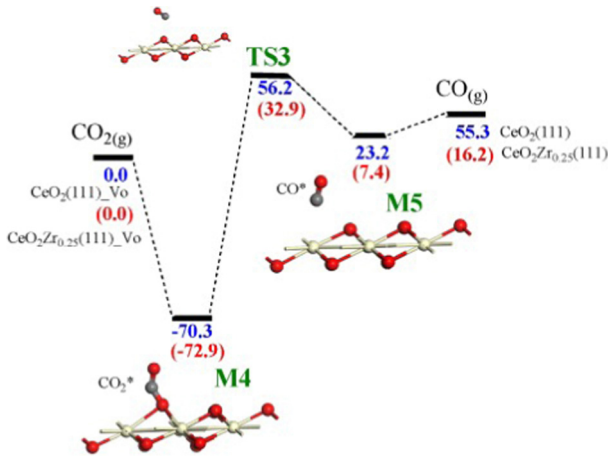

Fig. 5 Potential energy surfaces for the successive steps of CO_2 splitting calculated by DFT+U on CeO_2(111) and $Ce_{0.25}Zr_{0.75}O_2$(111) surfaces with an oxygen vacancy, V_O. Values of the energy barriers (in kJ mol^{-1}) are referenced to CO_2(g), and those in brackets refer to $Ce_{0.25}Zr_{0.75}O_2$(111). Only the three topmost layers are displayed. Reproduced from ref. 61 with permission from Elsevier.

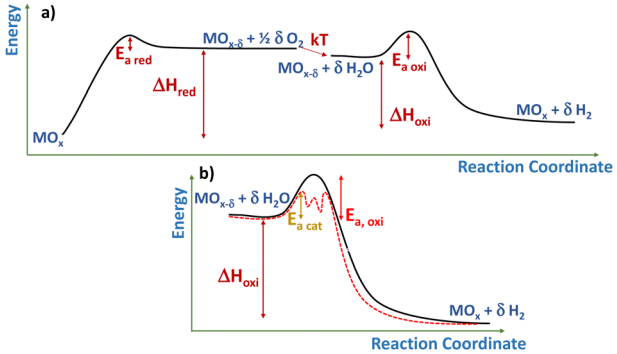

Fig. 6 Scheme of the energy landscape of (a) a two-stage thermochemical cycle over a generic non-stoichiometric oxide, MO_x and (b) detail the water splitting stage showing an alternative catalytic pathway. ΔH_{red} and ΔH_{oxi} represents, respectively, the reduction or oxidation enthalpy of the oxide, while $E_{a,red}$, $E_{a,oxi}$, and $E_{a,cat}$ are the activation energy of, respectively, the reduction, the oxidation and the oxidation in the presence of a catalyst.

the so far modest advances in this approach, exploring the possible avenues for improvement, and learning from the coupling of renewable power and catalysis are the main topics of this perspective. However, assessing the complex interplay between different active components simultaneously participating in different solid–gas reactions requires first establishing some clear definitions of what can be considered a catalyst in the context of thermochemical cycles. These fundamental aspects will be discussed in the next section.

Some working definitions: what does count as a heterogeneous catalyst in thermochemical cycles?

A catalyst can be simply described as a substance accelerating the reaction rate without modifying the thermodynamic equilibrium.[63] From a kinetic point of view, the catalytic effect implies the lowering of the activation energy barrier to the process by providing an alternative reaction pathway (see Fig. 6b). In this sense, redox oxides used in the thermochemical cycles, as described by eqn (1)–(3), can be considered loosely as catalysts. In fact, although this term is seldom utilized in the recent literature, some pioneering articles about thermochemical solar production referred to the active redox oxides as catalysts.[64] In this line, it can be argued that these solids provide a lower energy pathway (Fig. 6a) by interaction with the solid vacancies that allow CO_2 and water splitting at a significant rate, while the redox solid is recovered unchanged after completing the process.[65] Although considering an isolated cycle, the ratio between the solid oxygen carrier and the gas reagent is relatively high, and this value approaches the typical catalytic/reagent ratio when averaged in many cycles, as expected in practical applications.

The activity of catalysts can be expressed by their turnover frequency (TOF). Although specific operation conditions must be considered to accurately determine this parameter,[66] TOF is usually defined as the ratio between the rate of product formation, in moles per time unit, and the number of catalytic sites, expressed in mols. Therefore, this parameter presents reciprocal time (frequency) units. Although determining the nature and concentration of the active sites can be tricky,[65] this metric provides a quantitative way to compare conventional catalysis. In contrast, using TOF for establishing a direct meaningful comparison of thermochemical cycles with the equivalent catalytic process is more challenging, since the operation of chemical looping processes is intrinsically discontinuous. Therefore, the duration of a typical thermochemical cycle (from minutes to hours) is at least two orders of magnitude larger than for a typical catalytic one (seconds to milliseconds). Then, while TOF is often larger than 10 s^{-1} for catalytic processes, for chemical looping system, including solar thermochemical cycles, TOF is the range of ms^{-1}.[67] Thus, for example, for methane, dry reforming over $NiCo/Ce_{0.75}Zr_{0.25}O_2$ at 750 °C, the TOF for CO formation is 2.5 s^{-1}.[68] In contrast, the TOF of solar thermochemical CO production using reticulated CeO_2 is estimated to be about 1.1×10^{-4} s^{-1} (1.2×10^{-2} considering the peak rate) at 1250 °C. It is important to stress that these differences in the TOF are not necessarily due to a low instantaneous rate. In this way, it has been reported that chemical looping dry reforming of methane over $La_{0.9}Sr_{0.1}FeO_3/ZrO_2$ presents a higher activity for syngas production than conventional catalytic process under comparable isothermal conditions.[69] In fact, the remarkably lower TOF arises from the relatively high amount of redox oxide and the longer duration of the cycle. Therefore, increasing the frequency of the cycles can be a key parameter to optimize thermochemical fuel production.

Another relevant difference between these two gas–solid processes is that catalysis is intrinsically a surface phenomenon, while transformations of the solids in thermochemical cycles imply the whole material, so diffusion in the bulk of

relevant species such vacancies, oxide ions and electrons should also be considered. Accordingly, as mentioned in the previous section, some kinetic models specifically consider the diffusion of defects in the solid.[57]

For these two kinds of solid–gas processes a complete recovery of the solid in its initial state is expected, which allows continuous operation in both catalytic and thermochemical cycles, but in practice deactivation is an important concern. In the case of thermochemical cycles, structural and morphological degradation can arise due to the severity of the operation conditions that promote sintering and can induce structural in shaped solids during redox cycling. In fact, the durability of the oxygen carriers is an important issue when operating on large scale and under realistic conditions. For example, this is one of the main practical limitations of using Zn ferrites for solar thermochemical hydrogen productions.[37] Likewise, although CeO_2 has shown excellent cyclability at the lab scale,[14] plant operation have revealed minor structural integrity problems of the large ceramic foam components after completing 62 cycles.[17]

In the context of solarization of liquid fuels production, a recent thermodynamic study has compared the production of syngas from methane steam reforming by a conventional catalytic route with isothermal chemical looping, operating in both cases under 15 bar of pressure.[70] Considering the subsequent synthesis of methanol from the obtained solar syngas, the obtained results reveal that energy efficiency using CeO_2 as an oxygen carrier in the chemical looping was lower (0.70) than for the catalytic conversion (0.79) due to the higher operation temperature, which in addition should be carefully controlled to avoid carbon deposition caused by methane cracking under these conditions. A direct catalytic route can be in certain cases a more convenient alternative for driving solar thermochemical processes, although the impact on the carbon footprint of each possible process should be also evaluated. Yet, one of the key advantages of the chemical looping approach is that products are obtained separately in each stage, and this allows for easily tuning the H_2/CO ratio by adapting the composition of the feed.

With this background about the parallelisms and differences between the two types of processes, catalytic and thermochemical, in this perspective, we approach the use of conventional short-cycle heterogeneous catalysts to enhance longer-period thermochemical cycles. Although many of the redox oxides applied to thermochemical cycles also present relevant catalytic properties that can contribute to the overall activity, here we focus on the incorporation of additional metallic components in low amounts to promote the activity in any of the two stages. This criterion is intended to provide a clear cut definition for identifying these hybrid systems and to explore the potential synergetic effects between catalysis and thermochemical cycles. However, it should be kept in mind that as different reactions can occur simultaneously, cooperative (or competitive) interactions between components of the active solid are likely to happen. In this regard, the redox contribution of the catalytic active component to the thermochemical cycle can be generally disregarded because of its low concentration. Besides, following initial activation, catalytic metals are expected to remain in a reduced state under reaction conditions.[67]

Ascertaining potentially relevant interactions between components may need operando techniques, which are challenging to be applied at extremely high temperature. Accordingly, *in situ* studies designed to gather information at these harsh conditions are still scarce, although some recent reports have approached the *in situ* study of CO_2 splitting over CeO_2 at 800 °C.[71] Furthermore, synchrotron techniques are also increasingly applied to determine mechanistic and structural aspects of thermochemical cycles.[72]

In the following section, we discuss the rationale for using heterogeneous catalysts at high-temperature processes, setting the limits for the feasibility of their use.

Catalytic promotion of thermochemical cycles

Although the utilization of a catalytic element has received relatively little attention in thermochemical cycles based on redox oxides, in the case of sulfur-based cycles (sulfur–iodine or hybrid), the participation of a heterogeneous catalyst is crucial for achieving efficient hydrogen production.[20] This is because the key step of SO_3 reduction, which takes place according to the following reaction:

$$SO_3\ (g) \rightarrow SO_2\ (g) + 1/2\ O_2\ (g)\ \Delta H = 99\ kJ\ mol^{-1} \quad (4)$$

is too slow below 800 °C and, therefore, it requires the use of an appropriate catalyst for reaching a reasonable conversion. Typically, these catalysts consist of noble metals (usually Pt, Pd, or Rh) supported on oxides unreactive to SO_3 such as SiO_2 or TiO_2. These catalysts are efficient at relatively low temperatures, but they are prone to deactivation by sintering or volatilization of noble metal oxide species such as PtO_x, which are formed during reaction. Encapsulation of metal particles may mitigate this problem.[73] Alternatively, catalysts based on vanadates of rare earth or alkaline-earth elements supported on SiO_2 have gathered significant interest due to their lower cost and competitive catalytic activity, especially at temperatures around 800 °C.[74] Under these conditions, vanadates form partially melted phases, which have shown catalytic activity. However, despite the potential interest of these sulfur-based cycles, which can operate at milder temperatures than those using redox oxides, the intrinsic complexity of these multistep processes, which poses challenges for efficient heat recovery, and the difficulties of operating in corrosive atmospheres, sulfur-based thermochemical cycles are unlikely to be relevant contenders for solar fuels production in the short-term.

In contrast with the case of SO_3 decomposition, CO_2 or water splitting on reduced oxides involve a solid phase as a reactive species. This fact implies that optimization of the reaction rates should consider the contribution of both surface reactions and bulk processes such as vacancies diffusion.[75] Incorporation of catalytic metals is expected to affect only surface processes,

although cooperative interactions impacting the redox transformations of the solid can also be possible.

Pioneering work performed in 1980 showed an enormous boost in water splitting at a very low temperature, 200 °C, by incorporating Pd, Ni and particularly Pt on CeO_2 pre-reduced in hydrogen. This last metal increased the rate of hydrogen production by three orders of magnitude.[76] Even though these activation conditions are unlike those required for solar processing, this study confirmed the interest in the incorporation of catalytic active components to the redox oxide for enhancing the hydrogen yield. Likewise, addition of Rh to CeO_2 also resulted in an increment of the rate for the isothermal water splitting at 1500 °C, while the effect for oxygen evolution was limited.[77] However, the catalytic effect of Rh on hydrogen production is clearly enhanced (see Fig. 7) at temperatures below 1100 °C.[56] Thus, the maximum rate for hydrogen generation at 800 °C is almost double over Rh/CeO_2 than for CeO_2.

Remarkably, incorporation of Rh to CeO_2 as a catalyst has been used as a way to explore the validity of the thermo-kinetic model,[56] which assumes that for high enough temperatures, the rate of surface processes and bulk diffusion is fast enough to be disregarded. This is consistent with the experimentally observed overlapping of the hydrogen production curves for both Rh/CeO_2 and CeO_2 for assays performed above 1200 °C, as shown in Fig. 7. Therefore, this behavior suggests that there is a limited interval of temperatures for enhancing the thermochemical solar fuels production using a catalytic metal.

Recently, the impact of several noble metals, Ru, Pt and Ir, on the efficiency of CO_2 splitting over $Ce_{0.85}Zr_{0.15}O_2$ has been investigated by the Can Li group.[78] Dispersion of these metals on Zr-doped ceria prepared *via* wet impregnation slightly increases oxygen release, but CO_2 splitting is significantly promoted by PtO_x, and in a larger extent by IrO_x. Thus, for CO_2 splitting at 800 °C during a 60 min period, the total CO production using a catalyst with 0.4 atom% of IrO_x is two-fold that of unmodified $Ce_{0.85}Zr_{0.15}O_2$. If IrO_x is incorporated during the mixed oxide synthesis, using a solution combustion method, the obtained materials exceed the rate of CO production of the impregnated catalyst. Thus, the rate of CO evolution is 5.9 mL g^{-1} for the material loaded with 1 atom% of IrO_x for the first 10 min at 800 °C, which represents almost a threefold increment with regards to unmodified $Ce_{0.85}Zr_{0.15}O_2$. According to XPS results, IrO_x consists mainly of Ir^0 (*ca.* 80%) but with a significant contribution of Ir^{4+}. Optimal catalytic effect is observed at different metal loadings for materials prepared by combustion (of 1 atom%) or impregnation (0.4 atom%). These differences have been related to variations in the metal dispersion, induced by the preparation route. The role of IrO_x in boosting the activity is hypothesized to be due to an increase in the mixed (ionic and electronic) conductivity of Ce oxide, which favors oxygen vacancies formation and diffusion since these charge carriers participate actively in the process of vacancy formation and removal, which occurs through the equilibrium: $1/2O_2 + V_O + 2e^- \leftrightarrow O^{2-}$. In addition, Ir also plays an important role in easing the rupture of the C–O bond.[78] Catalytic enhancement of CO generation is significant in the 700–1000 °C interval and it reaches a maximum in the 800–900 °C range, depending on the Ir content. Although the total production of CO during the whole stage is comparable, the peak production rate is still significantly lower for $IrO_x/Ce_{0.85}Zr_{0.15}O_2$ than for CeO_2. This is because unmodified ceria shows a more favorable kinetic than the Zr-doped oxides, and this difference is not completely compensated by the promotion effect of the noble metal catalyst. Finally, it is important to note that although the catalytic promotion of IrO_x has proven to be preserved during a few cycles, it would be necessary to confirm the long-term stability of these multicomponent materials under realistic conditions.

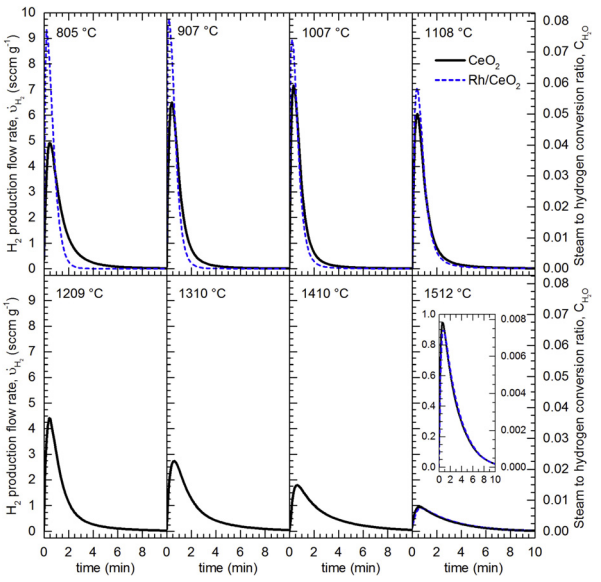

Fig. 7 Hydrogen release profiles obtained by water splitting at different temperatures (flow of 278 sccm of 20% H_2O in Ar) over CeO_2 (Black lines) and Rh/CeO_2 (Dashed blue lines) previously reduced in Ar at 1488 °C. Reproduced with permission from ref. 56 with permission from Elsevier.

Catalytic promotion without using any noble was verified on Cr-modified CeO_2 by the van Bokhoven group.[79] These materials present a remarkably faster rate for CO and hydrogen evolution than undoped oxides. The best results are obtained for the sample containing 15 atom% of Cr and prepared by incipient wetness impregnation. This material shows a rate of CO and H_2 production of, respectively, 2.50 and 1.94 mL g^{-1} min^{-1} at 800 °C, while for unmodified CeO_2, the corresponding rates for CO and H_2 are 0.005 and 0.09 mL g^{-1} min^{-1}, respectively. Furthermore, the rate of oxygen evolution up to 1500 °C in Ar atmosphere, 0.16 mL g^{-1} min^{-1}, is three times more than that of CeO_2. In these materials, formation of the perovskite $CeCrO_3$ is detected in the oxidized materials in a proportion of 7–10% depending on the preparation method. This phase appears to be inert for water and CO_2 splitting. However, considering the phase diagram of the Cr–O system, it is expected that metallic chromium can also be present following reduction at high temperatures and low oxygen pressure. Accordingly, the authors suggest that the promotion of CO formation can be explained by considering the catalytic role of Cr^0 in favoring CO_2 dissociation. In addition, these metallic centers may also

play a role in easing the hydrogen release, although the promotion of water splitting with Cr-modified CeO_2 is not as efficient as for CO_2 activation.

Similarly to the case of CeO_2, IrO_x has also been applied as catalyst to enhance CO_2 splitting over the perovskite $LaFeO_3$ by the Can Li group.[80] Likewise, differences in the promotion are also found depending on the preparation route. Solution-combustion method, which is expected to favor the incorporation of Ir into the perovskite lattice, is also in this system more effective than impregnation for promoting CO production. Thus, using the perovskite $LaFe_{0.9}Ir_{0.1}O_3$, which shows some segregation of IrO_x, the generation of CO increases about 50% at 1000 °C with regards to the unmodified ferrite during the first 10 minutes, and it is more than 30% larger, after 60 minutes of reaction, reaching a rate of 4.1 mL g^{-1}. In contrast, using an impregnated sample containing 0.7 atom% of Ir, CO_2 splitting yields only 3.8 mL g^{-1} in 60 minutes. Interestingly, for these perovskites, the influence of Ir on the oxygen evolution stage is much more relevant than for $Ce_{1-x}Zr_xO_2$ materials. Thus, the O_2 release for $LaFe_{0.9}Ir_{0.1}O_3$ is about double that for $LaFeO_3$ and the onset temperature of this process, 800 °C, is remarkably lower than for the unmodified ferrite (1250 °C). This has been related to the well-known capacity of IrO_2 of catalyzing the formation of O_2, which is exploited in electrochemical devices.[81] On the other hand, the stability of the CO generation on the Ir-modified materials was confirmed for 10 cycles and, although some decrease in the activity was observed, CO production remained higher than for $LaFeO_3$.

Incorporation of noble metal catalysts for enhancing the release of oxygen from perovskites has been also investigated to enhance the oxygen storage capacity. This concept could be also potentially transferred to the first stage of solar fuels production (eqn (1)). One notable example of the potential of metals to alter the redox properties of the oxide is the promotion of reduction of thin-films of the perovskite $SrCoO_3$ to the brownmillerite $SrCoO_{2.5}$ by Pt and Ag.[82] This process occurs at room temperature under vacuum, although it takes several hours. Nevertheless, in the case of high-temperature solar thermochemical processes, the application of relatively volatile metals such as Ag (melting point 961.78 °C) should be discarded.

Catalysis is very relevant for solarized processes such as chemical looping dry-reforming. This route can be considered to be in the interface of solar processes with conventional chemical looping and thermal catalysis, and it is currently attracting significant interest due to the high productivity of syngas achieved at more moderate temperatures.[83] However, this process can only be considered free of fossil carbon when biogas is the only methane source.[69,84–86] The use of exsolution synthesis to anchor metal nanoparticles with catalytic activity such as Ni, Fe, Co or Ru[87] into perovskites and CeO_2[88] is currently attracting high interest for this application as a consequence of the thermal stability these metal particles anchored to the redox oxide, which prevents their sintering at high operation temperatures. However, this route of syngas production will not be further discussed here since this study is focused on the production of fully renewable thermochemical fuels.

In brief, the positive effects of the incorporation of some noble and transition metals on redox oxides applied to CO_2 and water splitting have been experimentally confirmed. The most representative examples of this catalytic promotion of thermochemical fuel production are summarized in Table 2. However, results so far obtained show, in general, moderate improvements, especially at lower operation temperatures. Nevertheless, information available is still too scarce to assess the real opportunities of these bifunctional materials consisting of both redox and a catalytic component. In this regard, among other aspects, for practical utilization, it would be necessary to explore the stability of these heterogenous solids, performing more than 100 cycles, because phenomena such as encapsulation of the metal or phase segregation may limit their applicability in the long term.

Catalytic upgrading of thermochemical solar fuels

In addition to its role in boosting the elementary processes of the thermochemical cycles leading to oxygen releases and syngas formation, catalytic transformations are essential for upgrading solar syngas into more valuable molecules, yielding

Table 2 Most relevant catalytic systems used to promote thermochemical solar fuels production

Reaction	Material	Conditions	Promotion	Ref.
SO_3 reduction	$LaVO_4/SiO_2$	800 °C Direct. Sulfur cycle stage	Catalysts are always needed in sulfur-based cycles	74
WS	Rh/CeO_2	800–1100 °C Direct	Double rate than CeO_2 at 800 °C	55
CDS	1% $IrO_x/Ce_{0.85}Zr_{0.15}O_2$	700–1000 °C Direct	Threefold increment in the rate at 800 °C with regards to unmodified $Ce_{0.85}Zr_{0.15}O_2$.	78
OER/WS/CDS	15% Cr–CeO_2	800–1500 °C Direct	500-fold increment for CO and 30 for H_2 rates at 800 °C. Triple O_2 production at 1500 °C	79
OER/CDS	$LaFe_{0.9}Ir_{0.1}O_3$	800–1250 °C Direct	CO production rate one third larger at 1000 °C. Double production of O_2 than $LaFeO_3$	80
Methanation	1% Rh/CeO_2	350–500 °C Indirect	CH_4 generation at 500 °C	93

WS: water splitting, CDS: carbon dioxide splitting, OER: oxygen evolution reaction.

for example kerosene or other hydrocarbon fractions.[17,89] This can be uncoupled from the solar thermochemical cycle, as is the case in larger scale demonstration plants so far assayed,[89] by accumulating and subsequently processing the generated solar syngas. Then, selecting the catalyst and the operation conditions, either hydrocarbons, obtained by Fischer–Tropsch synthesis, or methanol can be produced.[17,89] Using the first procedure, a liquid fraction containing 16% kerosene (hydrocarbons with chain length in the C_{10}–C_{15} range), and 40% diesel (C_{15}–C_{20}) can be obtained operating at 30 bar and 210 °C using a feed with a H_2/CO ratio of 2.15. In addition, Fischer-Tropsch processing of syngas also yielded a wax phase, which has an additional 7% of kerosene and 40% of diesel. Furthermore, the Steinfeld group has shown the technical feasibility of producing fuels from just sunlight together with CO_2 and H_2O extracted from air in a 5 kW thermal pilot solar facility provided with a module for the capture of these gases from air, and a catalytic processing unit for liquid fuel production.[89] This system yields 12.81 liters of syngas per kg of ceria, with a H_2/(CO +CO_2) molar ratio of 2.7. In addition, to hydrocarbon production, this solar syngas was applied to methanol synthesis using a commercial Cu–ZnO–Al_2O_3 catalyst. This system achieved a conversion by a single pass of 27% in a recirculation reactor operating at 230 °C and 50 bar. This plant can produce jet fuel with an estimated cost of $1.2–2 per litre, although it has an overall sun-to-liquid energy efficiency of only about 0.8%, considering the energy consumption of all the units. However, it is expected that this value can be greatly improved by optimization of the design of the plant.

In order to set the limits of the economic viability, solar thermal plants to produce methanol, with separate units for thermochemical conversion, storage of the produced syngas and the synthesis of methanol have been modeled.[18] Assuming that the plants are installed in Almeria (SE Spain), this simulation indicates that with a heliostat field of about 88 hectares and a tower of 220 m, about 22 kt y^{-1} of methanol can be produced yearly at a cost of 1.14 $ per L. Further upgrading of the model, considering the implementation of an additional unit for the capture of CO_2, ideally powered by the waste heat of the plant, predicted the production of 11.8 kt y^{-1} with a cost of about 3€/l, despite considering a location, (Riyadh, Saudi Arabia), with higher direct irradiation.[90]

Despite these encouraging results for a sequential transformation, direct catalytic conversion in one step under solar thermal conditions of CO_2 and H_2O into simple hydrocarbons such as methane is attractive because that molecule is a more useful fuel than syngas and, in principle, a direct route can allow to increase the efficiency and simplify the system. However, one important obstacle to this end is that thermodynamics favors the production of hydrocarbons at much lower temperatures and higher pressures than those required for thermochemical CO_2 and water splitting.[91] However, despite these significant constraints to the maximum yield that can be achieved by direct catalytic promotion, several reports have experimentally explored the limits of this approach.

The feasibility of generating CH_4 directly from CO_2 and water was investigated by Haile's group by incorporating 10%wt. Ni on Sm-doped CeO_2.[92] Following reduction, this material allowed a significant production of CH_4 at 400 °C. According to thermodynamic expectations, the activity progressively decayed with increasing temperature, so only CO and H_2 are detected at 700 °C. However, in this report, the catalyst was reduced previously in hydrogen at 800 °C, and those conditions allow the achievement of higher non-stoichiometry than under usual solar conditions, and cycling stability was not investigated.

Thermochemical synthesis of CH_4 from CO_2 and water over Rh/CeO_2 was determined to be rather effective between 350 °C and 500 °C, while unmodified ceria yields only syngas.[93] In this case, the material was reduced at 1300 °C in an Ar stream, and using a H_2/CO ratio of 3 and a pressure of 1 Atms, the yield of methane is about 70% at 500 °C and it drops to about 40% at 600 °C. The reason for this behavior is that as the temperature raises reverse water gas shift, which is also promoted by Rh, becomes the predominant process.[91] Characterization of this material indicates that Rh is incorporated into the CeO_2 lattice with the formation of oxygen vacancies and it remains stable under the assayed conditions.

In a subsequent more detailed study, it was confirmed that 1 wt% Rh/CeO_2 was very effective for CH_4 generation from CO_2 and H_2O at 500 °C following thermal reduction at 1400 °C in Ar, as shown in Fig. 8.[94] In contrast, 10 wt%. Ni/CeO_2 is less active than the Rh catalyst for CH_4 generation at 500 °C following reduction in hydrogen at 600 °C, and it does not show any methanation activity under reduction at 1400 °C in an inert gas atmosphere. This fact has been attributed to the volatilization of Ni at these extreme temperature. In contrast, Rh/CeO_2 has proven to keep the activity for methane generation for 58 successive cycles, although a progressive decline of the activity is observed after the first 10 cycles. In addition, it is important to note that the selectivity to methane is low, and hydrogen and

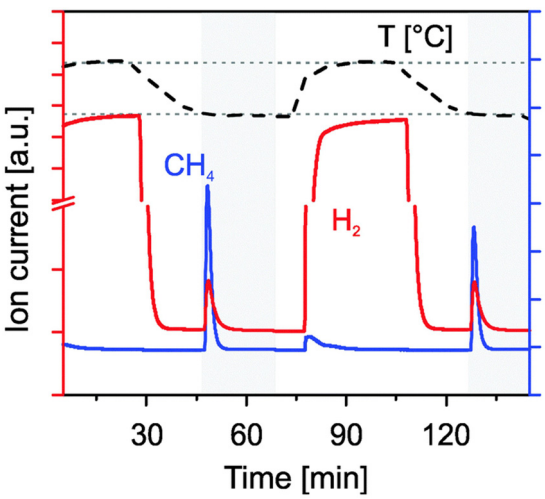

Fig. 8 Formation of hydrogen and methane at 500 °C from water (flow of 278 sccm of 20% H_2O in Ar) and carbon dioxide by reoxidation of Rh/CeO_2 previously reduced in H_2/Ar at 500 °C rhodium-doped ceria. Reproduced with permission from ref. 94 with permission from RSC.

CO are also simultaneously produced, although increasing the H_2O/CO_2 proportion raises the yield of methane.

On the other hand, continuous catalytic production of solar fuels under the fluctuating conditions imposed by renewable sources has been evaluated in the context of power-to-gas schemes fed by electrochemically generated hydrogen.[95] In this context, the effect of variable gas composition on the methanation of CO_2 over $Ni/CaO–Al_2O_3$ catalyst has been investigated by operando XAS spectroscopy.[96] In contrast, thermochemical solar fuel production has always relied on buffering the oscillations due to cyclic syngas production by accumulating the gas. This approach increases the reliability of the catalytic upgrading but makes less efficient the integration of the different units. Therefore, it can be worth exploring also in the case of solar thermal plants the feasibility of a more direct coupling of the solar receiver and the catalytic unit, considering the impact of the variability in the feed composition on fuel productivity.

These results, despite proving the technical feasibility of directly generating solar methane, clearly point out the technical challenges of coupling two processes that present optimal yields under very different conditions. However, the relatively low number of studies and catalyst compositions investigated, calls for additional research effort on optimizing thermochemical and catalytic upgrading processes operating in tandem.

Future outlook

Despite the promising developments in the last decade, the thermochemical route for solar fuel production has not reached yet the solar-to-fuel efficiency required for commercial development, which is estimated to be higher than 10% [2]. Reaching this threshold will imply additional research efforts for the development of redox materials with enhanced properties and solar plants with optimized design. Furthermore, thermochemical production of solar fuels critically relies on catalytic processes for converting the primarily produced syngas into high energy molecules such as methanol or different hydrocarbon fractions. Accordingly, finding ways to harmonically coupling these two processes, thermochemical and catalytic, in such a way to efficiently use solar energy also for powering catalytic transformations is of high practical interest. Despite the relatively modest progress so far obtained by hybridizing these technologies, prospects for further enhancement of the catalytic production of solar thermochemical fuels can be foreseen in different areas, as discussed below.

Operation at very high temperatures tends to speed-up the processes, and accordingly, direct catalytic promotion becomes irrelevant, as it has experimentally found.[56] However, there are still opportunities for achieving a reduction of the redox carriers at lower temperatures by incorporating an O_2 evolving catalyst and, more clearly for water and CO_2 reactions, which take place at lower temperatures, where catalytic promotion is expected to be relevant. In this respect, the moderate promotion observed by noble metals such as Ir could be further improved by using ex-solution synthesis that can stabilize metal particles and maximize the interaction with the metal oxide matrix. This strategy is currently applied to SOFC and other electrochemical devices, and for chemical looping dry reforming but to our knowledge it has not been explored for the direct catalytic enhancement of CO_2 or water splitting. On the other side, the use of redox active transition metals as dopants such as V or Cr among others, which present redox and catalytic properties, has already demonstrated efficacy for promoting the activity of CeO_2, and it can be worth exploring in more detail their possible benefits. Obviously, many other catalytic additives, yet untested, can be potentially used for boosting thermochemical cycles.

Further development of *in situ* and operando studies of these catalytic systems can be of high value not only from a fundamental point of view to understand the mechanisms at the molecular scale of these processes, but likewise to rationally improve them. However, the extreme operation temperatures impose significant limitations for some spectroscopies measurements, although XAS[97] and Raman[71] measurements are possible for redox systems at relevant conditions. Furthermore, *in situ* XRD, which provides information about phase evolution, can be also of interest for investigating thermochemical processes.[72]

In the case of indirect, two steps transformations to upgrade solar thermochemical fuels improving the design of the solar reactors working in tandem with a catalytic one is essential to manage the flows of heat and mass efficiently. This kind of consecutive reactor has been proposed for coupling sequential catalytic reactions such as for example the production of ethanol from syngas[98] or the recently proposed production of C_3 oxygenates from CO_2 and ethane.[99] The experience gained with these tandem reactors can give insights into how to maximize yields in solar applications.

With regards to efficiently use solar power, integration of thermochemical storage systems[100] can be a suitable approach to deal with the difference between the optimal operating temperatures for thermochemical and catalytic processes. However, extensive work on modeling and design will be necessary to exploit these multiunit systems efficiently. Besides, a moderate increase in the operation pressure could reduce the temperature gap between the production and the catalytic upgrading of syngas, and accordingly, this strategy can open a window for favorable operation conditions, which is worth exploring. This may also require the development of catalysts with high stability and adapted to these novel conditions. In addition, it would be necessary to further investigate how to optimize the operation under the fluctuating conditions imposed on the one hand by the thermochemical cycles and on the other hand by the inherent variability of solar flux.[101,102]

In summary, this panorama of the application of catalysis for promoting the production of solar thermochemical fuels has revealed that, despite the strong limitations dictated by the thermodynamics constraints, there are interesting opportunities to couple these two processes to maximize the efficiency in storing the solar energy in chemical bonds. So far, research

on coupling catalysis with thermochemical processes has been relatively scarce but it seems highly possible that the technological and scientific interest in this area will increase in the near future.

Author contributions

JMC: conceptualization, writing – original draft, and funding acquisition; AB: writing – review & editing, and funding acquisition.

Conflicts of interest

There are no conflicts to declare.

Acknowledgements

The authors appreciate the financial support from the ACES2030 program of the "Comunidad de Madrid" and European Structural Funds (P2018/EMT-4319). A. B. also thanks the "Talento" program of the "Comunidad de Madrid" for funding the project "SmartSolFuel".

References

1 D. Henner, REN21, Ren21, 2017.
2 H. Song, S. Luo, H. Huang, B. Deng and J. Ye, *ACS Energy Lett.*, 2022, **7**, 1043–1065.
3 Y. Zhao, W. Gao, S. Li, G. R. Williams, A. H. Mahadi and D. Ma, *Joule*, 2019, **3**, 920–937.
4 A. M. Oliveira, R. R. Beswick and Y. Yan, *Curr. Opin. Chem. Eng.*, 2021, **33**, 100701.
5 M. M. May and K. Rehfeld, *Adv. Energy Mater.*, 2022, **12**, 2103801.
6 J. Jia, L. C. Seitz, J. D. Benck, Y. Huo, Y. Chen, J. Wei, D. Ng, T. Bilir, J. S. Harris and T. F. Jaramillo, *Nat. Commun.*, 2016, **7**, 13237.
7 H. Chen, L. Song, S. Ouyang, J. Wang, J. Lv and J. Ye, *Adv. Sci.*, 2019, **6**, 1900465.
8 J. Schneidewind, *Adv. Energy Mater.*, 2022, **12**, 2200342.
9 C. Ros, T. Andreu and J. R. Morante, *J. Mater. Chem. A*, 2020, **8**, 10625–10669.
10 W. H. Cheng, M. H. Richter, M. M. May, J. Ohlmann, D. Lackner, F. Dimroth, T. Hannappel, H. A. Atwater and H. J. Lewerenz, *ACS Energy Lett.*, 2018, **3**, 1795–1800.
11 J. Liu, Y. Liu, N. Liu, Y. Han, X. Zhang, H. Huang, Y. Lifshitz, S. T. Lee, J. Zhong and Z. Kang, *Science*, 2015, **347**, 970–974.
12 P. Zhou, I. A. Navid, Y. Ma, Y. Xiao, P. Wang, Z. Ye, B. Zhou, K. Sun and Z. Mi, *Nature*, 2023, **613**, 66–70.
13 A. Iglesias-Juez, F. Fresno, J. M. Coronado, J. Highfield, A. M. Ruppert and N. Keller, *Curr. Opin. Green Sustain. Chem.*, 2022, **37**, 100652.
14 D. Marxer, P. Furler, M. Takacs and A. Steinfeld, *Energy Environ. Sci.*, 2017, **10**, 1142–1149.
15 W.-H. H. Cheng, A. De La Calle, H. A. Atwater, E. B. Stechel and C. Xiang, *ACS Energy Lett.*, 2021, **6**, 3113.
16 M. Romero and A. Steinfeld, *Energy Environ. Sci.*, 2012, **5**, 9234–9245.
17 S. Zoller, E. Koepf, D. Nizamian, M. Stephan, A. Patané, P. Haueter, M. Romero, J. González-Aguilar, D. Lieftink, E. de Wit, S. Brendelberger, A. Sizmann and A. Steinfeld, *Joule*, 2022, **6**, 1606–1616.
18 N. Monnerie, P. G. Gan, M. Roeb and C. Sattler, *Int. J. Hydrogen Energy*, 2020, **45**, 26117–26125.
19 A. Bayón, V. A. De La Penã O'Shea, D. P. Serrano and J. M. Coronado, *J. CO2 Util.*, 2020, **42**, 101264.
20 C. Sattler, M. Roeb, C. Agrafiotis and D. Thomey, *Sol. Energy*, 2017, **156**, 30–47.
21 S. Abanades and G. Flamant, *Sol. Energy*, 2006, **80**, 1611–1623.
22 W. C. Chueh, C. Falter, M. Abbott, D. Scipio, P. Furler, S. M. Haile and A. Steinfeld, *Science*, 2010, **330**, 1797–1801.
23 S. S. Naghavi, A. A. Emery, H. A. Hansen, F. Zhou, V. Ozolins and C. Wolverton, *Nat. Commun.*, 2017, **8**, 1–6.
24 Y. Hao, C. K. Yang and S. M. Haile, *Chem. Mater.*, 2014, **26**, 6073–6082.
25 J. R. Scheffe, R. Jacot, G. R. Patzke and A. Steinfeld, *J. Phys. Chem. C*, 2013, **117**, 24104–24110.
26 A. J. Carrillo, J. L. M. Rupp and J. M. Coronado, *Energy Storage and Conversion Materials*, The Royal Society of Chemistry, 2020, pp. 136–187.
27 M. Kubicek, A. H. Bork and J. L. M. Rupp, *J. Mater. Chem. A*, 2017, **5**, 11983–12000.
28 J. R. Scheffe, D. Weibel and A. Steinfeld, *Energy Fuels*, 2013, **27**, 4250–4257.
29 M. Ezbiri, M. Takacs, D. Theiler, R. Michalsky and A. Steinfeld, *J. Mater. Chem. A*, 2017, **5**, 4172–4182.
30 A. H. McDaniel, E. C. Miller, D. Arifin, A. Ambrosini, E. N. Coker, R. O'Hayre, W. C. Chueh, J. Tong, W. C. Chueh and J. Tong, *Energy Environ. Sci.*, 2013, **6**, 2424–2428.
31 X. Qian, J. He, E. Mastronardo, B. Baldassarri, W. Yuan, C. Wolverton and S. M. Haile, *Matter*, 2021, **4**, 688–708.
32 D. R. Barcellos, M. D. Sanders, J. Tong, A. H. Mcdaniel and R. P. O'hayre, *J. Energy Environ. Sci*, 2018, **11**, 3256.
33 A. H. Bork, M. Kubicek, M. Struzik and J. L. M. Rupp, *J. Mater. Chem. A*, 2015, **3**, 15546–15557.
34 A. H. Bork, A. J. Carrillo, Z. D. Hood, B. Yildiz and J. L. M. Rupp, *ACS Appl. Mater. Interfaces*, 2020, **12**, 32622–32632.
35 A. A. Emery, J. E. Saal, S. Kirklin, V. I. Hegde and C. Wolverton, *Chem. Mater.*, 2016, **28**, 5621–5634.
36 A. Bayon, A. de la Calle, K. K. Ghose, A. Page and R. McNaughton, *Int. J. Hydrogen Energy*, 2020, **45**, 12653–12679.
37 M. Roeb, J. P. Säck, P. Rietbrock, C. Prahl, H. Schreiber, M. Neises, L. de Oliveira, D. Graf, M. Ebert, W. Reinalter, M. Meyer-Grünefeldt, C. Sattler, A. Lopez, A. Vidal, A. Elsberg, P. Stobbe, D. Jones, A. Steele, S. Lorentzou, C. Pagkoura, A. Zygogianni, C. Agrafiotis and A. G. Konstandopoulos, *Sol. Energy*, 2011, **85**, 634–644.
38 R. R. Bhosale, A. Kumar, F. AlMomani, U. Ghosh, P. Sutar, G. Takalkar, A. Ashok and I. Alxneit, *Ceram. Int.*, 2017, **43**, 5150–5155.

39 S. Zhai, J. Rojas, N. Ahlborg, K. Lim, M. F. Toney, H. Jin, W. C. Chueh and A. Majumdar, *Energy Environ. Sci.*, 2018, **11**, 2172–2178.
40 X. Zhai, F. Ding, Z. Zhao, A. Santomauro, F. Luo and J. Tong, *Commun. Mater.*, 2022, **3**, 42.
41 E. Mastronardo, X. Qian, J. M. Coronado and S. M. Haile, *J. Mater. Chem. A*, 2020, **8**, 8503–8517.
42 A. Bayon, A. de la Calle, E. B. Stechel and C. Muhich, *Energy Technol.*, 2022, **10**, 2100222.
43 J. Lou, Z. Tian, Y. Wu, X. Li, X. Qian, S. M. Haile and Y. Hao, *Sol. Energy*, 2022, **241**, 504–514.
44 C. L. Muhich, S. Blaser, M. C. Hoes and A. Steinfeld, *Int. J. Hydrogen Energy*, 2018, **43**, 18814–18831.
45 A. de la Calle, I. Ermanoski and E. B. Stechel, *Int. J. Hydrogen Energy*, 2022, **47**, 10474–10482.
46 S. Li, V. M. Wheeler, P. B. Kreider and W. L. Lipiński, *Energy Fuels*, 2018, **32**(10), 10838–10847.
47 B. Bulfin, F. Call, J. Vieten, M. Roeb, C. Sattler and I. V. Shvets, *J. Phys. Chem. C*, 2016, **120**, 2027–2035.
48 A. Le Gal, S. Abanades and G. Flamant, *Energy Fuels*, 2011, **25**, 4836–4845.
49 D. Arifin and A. W. Weimer, *Sol. Energy*, 2018, **160**, 178–185.
50 D. Arifin, A. Ambrosini, S. A. Wilson, B. Mandal, C. L. Muhich and A. W. Weimer, *Int. J. Hydrogen Energy*, 2020, **45**, 160–174.
51 B. Bulfin, A. J. Lowe, K. A. Keogh, B. E. Murphy, O. Lübben, S. A. Krasnikov and I. V. Shvets, *J. Phys. Chem. C*, 2013, **117**, 24129–24137.
52 L. J. Venstrom, R. M. De Smith, R. Bala Chandran, D. B. Boman, P. T. Krenzke and J. H. Davidson, *Energy Fuels*, 2015, **29**, 8168–8177.
53 H. Il, Ji, T. C. Davenport, M. J. Ignatowich and S. M. Haile, *Phys. Chem. Chem. Phys.*, 2017, **19**, 7420–7430.
54 H. Il, Ji, T. C. Davenport, C. B. Gopal and S. M. Haile, *Phys. Chem. Chem. Phys.*, 2016, **18**, 21554–21561.
55 M. J. Ignatowich, A. H. Bork, T. C. Davenport, J. L. M. Rupp, C. K. Yang, Y. Yamazaki and S. M. Haile, *MRS Commun.*, 2017, **7**, 873–878.
56 T. C. Davenport, M. Kemei, M. J. Ignatowich and S. M. Haile, *Int. J. Hydrogen Energy*, 2017, **42**, 16932–16945.
57 Z. Zhao, M. Uddi, N. Tsvetkov, B. Yildiz and A. F. Ghoniem, *J. Phys. Chem. C*, 2016, **120**, 16271–16289.
58 S. G. Rudisill, L. J. Venstrom, N. D. Petkovich, T. Quan, N. Hein, D. B. Boman, J. H. Davidson and A. Stein, *J. Phys. Chem. C*, 2013, **117**, 1692–1700.
59 H. A. Hansen and C. Wolverton, *J. Phys. Chem. C*, 2014, **118**, 27402–27414.
60 D. Marrocchelli and B. Yildiz, *J. Phys. Chem. C*, 2012, **116**, 2411–2424.
61 S. E. Rawadieh, M. Altarawneh, I. S. Altarawneh, M. A. Batiha and L. A. Al-Makhadmeh, *Mol. Catal.*, 2020, **498**, 111256.
62 K. Razmgar, T. Shittu, I. Oluwoye, A. Khaleel, G. Senanayake and M. Altarawneh, *J. CO2 Util.*, 2023, **67**, 102339.
63 E. Roduner, *Chem. Soc. Rev.*, 2014, **43**, 8226–8239.
64 A. Le Gal and S. Abanades, *Int. J. Hydrogen Energy*, 2011, **36**, 4739–4748.
65 G. B. Marin, V. V. Galvita and G. S. Yablonsky, *J. Catal.*, 2021, **404**, 745–759.
66 S. Kozuch and J. M. L. Martin, *ACS Catal.*, 2012, **2**, 2787–2794.
67 M. S. C. Chan, E. Marek, S. A. Scott and J. S. Dennis, *J. Catal.*, 2018, **359**, 1–7.
68 M. A. Vasiliades, C. M. Damaskinos, P. Djinović, A. Pintar and A. M. Efstathiou, *Catal. Commun.*, 2021, **149**, 106237.
69 D. Sastre, C. Á. Galván, P. Pizarro and J. M. Coronado, *Fuel*, 2022, **309**, 122122.
70 B. Bulfin, S. Ackermann, P. Furler and A. Steinfeld, *Sol. Energy*, 2021, **215**, 169–178.
71 E. Sediva, A. J. Carrillo, C. E. Halloran and J. L. M. Rupp, *ACS Appl. Energy Mater.*, 2021, **4**, 1474–1483.
72 S. Shulda, R. T. Bell, N. A. Strange, L. Metzroth, K. N. Heinselman, S. Sainio, S. Roychoudhury, D. Prendergast, A. H. McDaniel and D. S. Ginley, *Front. Energy Res.*, 2022, **10**, 1–18.
73 H. A. Khan, M. I. Iqbal, A. Jaleel, I. Abbas, S. A. Abbas and K. Deog-Jung, *Int. J. Hydrogen Energy*, 2019, **44**, 2312–2322.
74 M. Machida, A. Ikematsu, A. S. M. M. Nur and H. Yoshida, *ACS Appl. Energy Mater.*, 2021, **4**, 1696–1703.
75 H. Chang, E. Bjørgum, O. Mihai, J. Yang, H. L. Lein, T. Grande, S. Raaen, Y. A. Zhu, A. Holmen and D. Chen, *ACS Catal.*, 2020, **10**, 3707–3719.
76 K. Otsuka, M. Hatano and A. Morikawa, *J. Catal.*, 1983, **79**, 493–496.
77 Y. Hao, C. K. Yang and S. M. Haile, *Phys. Chem. Chem. Phys.*, 2013, **15**, 17084–17092.
78 Z. Chen, Q. Jiang, H. An, J. Zhang, S. Hao, X. Li, L. Cai, W. Yu, K. You, X. Zhu and C. Li, *ACS Catal.*, 2022, **12**, 7719–7736.
79 S. Mostrou, R. Büchel, S. E. Pratsinis and J. A. van Bokhoven, *Appl. Catal. A Gen.*, 2017, **537**, 40–49.
80 Q. Jiang, Z. Chen, J. Tong, M. Yang, Z. Jiang and C. Li, *ACS Catal.*, 2016, **6**(2), 1172–1180.
81 V. K. Puthiyapura, S. Pasupathi, H. Su, X. Liu, B. Pollet and K. Scott, *Int. J. Hydrogen Energy*, 2014, **39**, 1905–1913.
82 K. Wang, C. Han, Z. Shao, J. Qiu, S. Wang, S. Liu, K. Wang, C. Han, Z. P. Shao, S. M. Liu, J. S. Qiu and S. B. Wang, *Adv. Funct. Mater.*, 2021, **31**, 2102089.
83 S. Bhattar, M. A. Abedin, S. Kanitkar and J. J. Spivey, *Catal. Today*, 2021, **365**, 2–23.
84 O. Kwon, R. Huang, T. Cao, J. M. Vohs and R. J. Gorte, *Catal. Today*, 2021, **382**, 142–147.
85 S. Joo, A. Seong, O. Kwon, K. Kim, J. H. Lee, R. J. Gorte, J. M. Vohs, J. W. Han and G. Kim, *Sci. Adv.*, 2020, **6**, 1–9.
86 X. Gao, G. Liu, Y. Zhu, P. Kreider, A. Bayon, T. Gengenbach, T. Lu, Y. Liu, J. Hinkley, W. Lipiński and A. Tricoli, *Nano Energy*, 2018, **50**, 347–358.
87 F. Schrenk, L. Lindenthal, H. Drexler, G. Urban, R. Rameshan, H. Summerer, T. Berger, T. Ruh, A. K. Opitz and C. Rameshan, *Appl. Catal., B*, 2022, **318**, 121886.

88 A. J. Carrillo, L. Navarrete, M. Laqdiem, M. Balaguer and J. M. Serra, *Mater. Adv.*, 2021, **2**, 2924.
89 R. Schäppi, D. Rutz, F. Dähler, A. Muroyama, P. Haueter, J. Lilliestam, A. Patt, P. Furler and A. Steinfeld, *Nature*, 2022, **601**, 63–68.
90 E. Prats-Salvado, N. Monnerie and C. Sattler, *Energies*, 2021, **14**, 4818.
91 J. Gao, Y. Wang, Y. Ping, D. Hu, G. Xu, F. Gu and F. Su, *RSC Adv.*, 2012, **2**, 2358–2368.
92 W. C. Chueh and S. M. Haile, *ChemSusChem*, 2009, **2**, 735–739.
93 F. Lin, A. Wokaun and I. Alxneit, *Energy Procedia*, 2015, **69**, 1790–1799.
94 F. Lin, M. Rothensteiner, I. Alxneit, J. A. Van Bokhoven and A. Wokaun, *Energy Environ. Sci.*, 2016, **9**, 2400–2409.
95 D. A. Kuznetsov, B. Han, Y. Yu, R. R. Rao, J. Hwang, Y. Román-Leshkov and Y. Shao-Horn, *Joule*, 2018, **2**, 225–244.
96 B. Mutz, H. W. P. Carvalho, S. Mangold, W. Kleist and J. D. Grunwaldt, *J. Catal.*, 2015, **327**, 48–53.
97 A. J. Carrillo, L. E. Chinchilla, A. Iglesias-Juez, S. Gutiérrez-Rubio, D. Sastre, P. Pizarro, A. B. Hungría and J. M. Coronado, *Small Methods*, 2021, **5**, 2100550.
98 C. C. Amoo, C. Xing, N. Tsubaki and J. Sun, *ACS Cent. Sci.*, 2022, **8**, 1047–1062.
99 Z. Xie, Y. Xu, M. Xie, X. Chen, J. H. Lee, E. Stavitski, S. Kattel and J. G. Chen, *Nat. Commun.*, 2020, **11**, 1–8.
100 A. Lidor, Y. Aschwanden, J. Häseli, P. Reckinger, A. Steinfeld, A. Lidor, Y. Aschwanden, J. Häseli and P. Haueter, *Appl. Energy*, 2023, **329**, 120211.
101 U. Ash-Kurlander, O. Martin, L. D. Fontana, V. R. Patil, M. Bernegger, C. Mondelli, J. Pérez-Ramírez and A. Steinfeld, *Energy Technol.*, 2016, **4**, 565–572.
102 A. de la Calle and A. Bayon, *Int. J. Hydrogen Energy*, 2019, **44**, 1409–1424.

